Solar Energy Materials & Solar Cells 122 (2014) 183–189

Contents lists available at ScienceDirect

Solar Energy Materials & Solar Cells

journal homepage: www.elsevier.com/locate/solmat

Enhanced visible light responsive MWCNT/TiO_2 core–shell nanocomposites as the potential photocatalyst for reduction of CO_2 into methane

Meei Mei Gui [a], Siang-Piao Chai [a,*], Bo-Qing Xu [c], Abdul Rahman Mohamed [b]

[a] Low Carbon Economy (LCE) Group, Chemical Engineering Discipline, School of Engineering, Monash University, Jalan Lagoon Selatan, 46150 Bandar Sunway, Selangor, Malaysia
[b] Low Carbon Economy (LCE) Group, School of Chemical Engineering, Universiti Sains Malaysia, Engineering Campus, Seri Ampangan, 14300 Nibong Tebal, Pulau Pinang, Malaysia
[c] Innovative Catalysis Program, Key Lab of Organic Optoelectronics & Molecular Engineering, Department of Chemistry, Tsinghua University, Beijing 100084, China

ARTICLE INFO

Article history:
Received 15 May 2013
Received in revised form
22 November 2013
Accepted 27 November 2013
Available online 31 December 2013

Keywords:
$MWCNT/TiO_2$
Core–shell
Nanocomposites
Photocatalysis
CO_2 photoreduction
Visible light

ABSTRACT

This work demonstrates the synthesis of $MWCNT/TiO_2$ core–shell nanocomposites and their application for photocatalytic reduction of CO_2 under visible light irradiation. $MWCNT/TiO_2$ core–shell nanocomposites were obtained from a newly developed coating approach. UV–vis analysis revealed that the photoactivity of the nanocomposites in the visible light range was significantly enhanced with the absorption edge extended to the visible light region (>400 nm). The XRD and Raman analysis indicated that the TiO_2 shell layer was composed of anatase TiO_2 nanocrystallite prevailing grew along the (1 0 1) direction. The $MWCNT/TiO_2$ core–shell nanocomposites exhibited conversion of CO_2 into methane in a continuous process under a low power visible light irradiation at atmospheric pressure. The highest methane yield of *ca.* 0.17 μmol/g-catalyst/h was recorded at the 6th hour of irradiation time.

1. Introduction

TiO_2 is the principle catalyst for almost all types of photocatalysis reaction. However, it is only photoactive at the wavelengths of below 400 nm due to its relatively large bandgap energy ($\sim$3.2 eV). In order for TiO_2 to be used for visible light applications, TiO_2 is usually modified with the addition of metal dopants or compounds that are photoactive in the visible light region, such as ruthenium dye, carbon materials, CdS, Cu, Fe, and so on [1,2]. In respect of being a high performance photocatalyst for CO_2 reduction under visible light illumination, modification of the TiO_2 is required to achieve the following important characteristics, namely: (i) easily to be photoactivated with lower bandgap energy; (ii) ability to absorb light in the visible range ($\lambda > 400$ nm); and (iii) ability to absorb CO_2 and water (sacrificial agent) on the catalytic surface [3].

Carbon nanotubes (CNTs), owing to their excellent optical properties and electron transfer ability, have been widely reported as an important substrate that can improve the photoactivity of TiO_2 [4]. In general, CNTs play two important roles in a photocatalyst: as photosensitizer that enables the photoactivation of TiO_2 under visible light irradiation and as electron sinks that transfer the electrons away from the TiO_2 particles after photoexcitation *via* the CNT–TiO_2 heterojunction. These electrons can subsequently trigger the photoreaction by formation of reactive radicals such as superoxide radical ions ($O_2^{\bullet -}$) and hydroxyl radicals ($HO^{\bullet}$) [5,6].

CNTs–TiO_2 composites exhibit great photocatalytic activity with excellent visible light absorption and unique electron charge transfer ability [7]. These composites were obtained most commonly using sol–gel [8–13] and other approaches such as chemical vapor deposition [14,15], functionalization with titanium precursor [16], and solvothermal [17]. The main concern of these earlier studies focused on improving the uniformity dispersion of the TiO_2 particles over the CNTs to yield the structure with minimum TiO_2 agglomeration. The control of the TiO_2 particle sizes and their dispersion over the CNTs was strongly dependent on the methods employed during the synthesis process, which was usually hard to be achieved.

In this work, the composite materials consisting of multi-walled carbon nanotubes (MWCNTs) and TiO_2 have been developed *via* core–shell coating, in which the MWCNTs are wrapped

* Corresponding author. Tel.: +603 55146234; fax: +603 55146207.
E-mail address: chai.siang.piao@monash.edu (S.-P. Chai).

0927-0248/$ - see front matter © 2013 Elsevier B.V. All rights reserved.
http://dx.doi.org/10.1016/j.solmat.2013.11.034

up by TiO_2 overlayers (shell). The MWCNT core induces visible light absorption and provides high surface area to accommodate the TiO_2 particles in the shell, making the MWCNT/TiO_2 nanocomposites highly active for photoreduction of CO_2. To the best of our knowledge, the performance of MWCNT/TiO_2 core–shell nanocomposites for CO_2 photoreduction has not been reported yet.

2. Materials and experiment procedures

2.1. Preparation of MWCNT/TiO_2 core–shell nanocomposites

Pristine MWCNTs used in this study were produced from Co-Mo/MgO catalyst using a rotary reactor, whose purity by the content of carbon was *ca.* 66.82% [18]. Prior to TiO_2 coating, the pristine MWCNTs were treated with acid to remove metal catalysts as well as to introduce carboxyl groups on the MWCNT surface to ease the coating process at the later stage. The acid treatment was done by continuously stirring of 500 mg of MWCNTs in a mixture of nitric acid (Chemolab supplies, 70%) and sulphuric acid (Chemolab supplies, 95–97%) mixed at a volume ratio of 1:3 at the concentration of 5 M each under reflux at 100 °C for 3 h. The mixture was then filtered and repeatedly washed with distilled water until neutral pH was achieved. The acid-treated MWCNTs were collected and dried overnight in oven at 80 °C.

In the second step, MWCNT/TiO_2 nanocomposites were synthesized by core–shell coating of TiO_2 (shell) on MWCNTs (core) surface. The TiO_2 core–shell coating was carried out using titanium butoxide (TBOT, Sigma Aldrich, 97%) as the titanium precursor, deionized water as the hydrolysis agent, and ethanol (Chemolab supplies, 96%) as the solvent for TBOT. Prior to the coating with TBOT solution, 0.16 g of acid-treated MWCNTs were sonicated in 20 mL of ethanol and water for 10 min. Next, the TBOT predissolved in 10 mL of ethanol was added into the MWCNTs-ethanol solution. The overall mixture was controlled at a TBOT: water:ethanol ratio of 1:5:50 (mol/mol). The mixture was continuously stirred in ice bath for an hour, followed by vacuum filtration and repeatedly washing with ethanol to remove TBOT in excess. The powder sample was collected and dried overnight in oven at 80 °C to remove excess ethanol. MWCNT/TiO_2 core–shell nanocomposites were obtained by calcination of the sample in air at 400 °C for 2 h. Anatase TiO_2 powder sample was also synthesized using the same procedure but without presence of MWCNTs and was used for comparison purpose.

2.2. Characterization of MWCNT/TiO_2 nanocomposites

The characteristics of the nanocomposites obtained were investigated before they were used for CO_2 photoreduction reaction. UV–vis spectroscopy (Agilent, Cary 100) equipped with powder cell holder (2.3 cm × 1 cm (diameter × cell depth); DRA-CA-301) was engaged to study the light absorption performance of the MWCNT/TiO_2 nanocomposites. Surface morphology of the nanocomposites was investigated *via* field emission scanning electron microscopy (FESEM, Hitachi SU8010) and high resolution transmission electron microscopy (HRTEM, JEM 2100f). Elemental analysis was performed by energy-dispersive X-ray spectroscopy (EDS) equipped with the FESEM. X-ray Diffraction (XRD) analysis and Raman spectroscopy with laser excitation at 532 nm (Renishaw inVia) were employed to study the crystal structure of the developed nanocomposites. Fourier-transformed infrared (FT-IR) spectra were obtained on a Nicolet iS10 FT-IR spectrometer using Kbr Die Model 129 to identify the intermediate products formed on the surface of the photocatalysts after the CO_2 photoreduction.

2.3. Photocatalytic reaction procedures

Photocatalytic activity of the MWCNT/TiO_2 core–shell catalysts was tested in a CO_2 photoreduction system with a continuous CO_2 flow at atmospheric pressure. The reaction was carried out under visible light irradiation with 15 W energy saving light bulb (Philips, TORNADO 15 W WW E27 220–240 V 1CT) [15]. The MWCNT/TiO_2 nanocomposites were coated on glass rods to ensure uniform and maximum exposure of the catalyst surface to the irradiated light. The coating of MWCNT/TiO_2 nanocomposites on the glass rods was carried out by mixing the powder sample with polyethylene glycol (PEG) (MW: 200, Merck) at a pre-calculated ratio of 1:3 (g:ml). The coating was done using a dip-coating method. Subsequently, the PEG was removed by thermal decomposition in air [19] at 300 °C for 30 min, leaving behind the coated layer of MWCNT/TiO_2 on the glass rods as shown in Fig. S1 (Supplementary materials). The coated glass rods were then loaded into quartz tubes with the dimensions of 10 mm × 200 mm (OD × length) which functioned as a photoreactor. Upon loaded with the glass rods, the photoreactor was flowed with CO_2 gas in dark for 30 min at a flowrate of 30 mL/min. Next, the light source was turned on and the CO_2 photoreduction was carried out with a controlled flowrate of the CO_2 gas. Water was used as the sacrificial reagent for the photoreduction reaction and was introduced into the reactor *via* bubbling of the CO_2 gas in water at room temperature. The entire photoreduction system was enclosed in a black box to avoid incoming irradiation light from the surrounding. During the CO_2 photoreduction reaction, the product gas was collected in gas bags from time to time (with the sampling time of 1 h) and the composition of the product gas was analyzed in a gas chromatography (GC) (Agilent 7890 A, Hayesep *Q* and mol sieve column) equipped with both TCD and FID. A schematic diagram of the photoreduction was shown in Fig. S2 (Supplementary materials). Methane concentration was quantified from the peak area of the GC spectra using the internal standard reference method.

The yield of methane was calculated using the following expression:

$$\text{Methane yield} = \frac{\text{Amount of methane produced}/h\ (\mu\text{mol}/h)}{\text{Amount of photocatalyst used}\ (g)} \quad (1)$$

3. Results and discussion

3.1. Characterization of the nanocomposites

Fig. 1 shows the UV–vis spectra of the MWCNT/TiO_2 core–shell nanocomposites compared to the acid-treated MWCNTs and anatase TiO_2 powder. The light absorption of the MWCNT/TiO_2 core–shell nanocomposites was found to have a similar trend with that of the anatase TiO_2 but at a magnified scale with absorption in visible light range (at 400–800 nm). The total light absorption of the MWCNT/TiO_2 nanocomposites was believed to be contributed by both TiO_2 and MWCNTs of which TiO_2 led to the light absorption in the UV range (200–400 nm) and the MWCNTs contributed to the light absorption over the whole UV–vis range (200–800 nm) [14]. MWCNT/TiO_2 nanocomposites have shown reduced absorption intensity compared to the acid-treated MWCNTs. This result is in agreement with the earlier literature [9,20,21]. The reduction of absorption intensity in the visible range of the nanocomposites can be attributed to the wrapping of TiO_2 shell over the MWCNT core which reduced the light intensity reaching at the MWCNT core [22]. The red shift of the absorption edge (> 400 nm) of the MWCNT/TiO_2 core–shell structure also implies an ability of the nanocomposites to be photoactivated under the visible light irradiation [13].

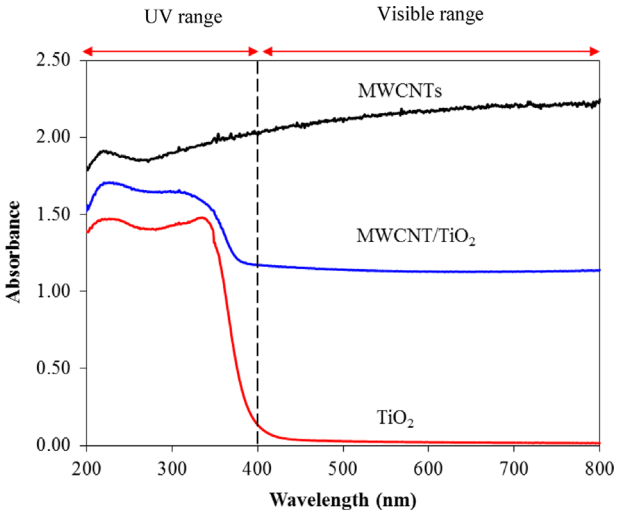

Fig. 1. UV–vis spectra of core–shell MWCNT/TiO_2, acid-treated MWCNTs and anatase TiO_2.

The surface morphology of the MWCNT/TiO_2 core–shell nanocomposites was examined with FESEM (Fig. 2a and b). The TiO_2 nanoparticles were visualized to deposit uniformly over the surface of MWCNTs, forming a TiO_2 shell that wrapped up around MWCNT with insignificant TiO_2 agglomeration. The diameters of the nanocomposites were measured to be in the range of *ca.* 40–60 nm, which were thicker than the diameter of acid-treated MWCNTs that ranging from *ca.* 31 to 35 nm. The presence of the TiO_2 shell was further confirmed by performing the EDS on the core–shell structure as shown in Fig. 2c.

HRTEM was carried out to investigate the internal structure of the core–shell nanocomposites. Fig. 3a shows the HRTEM image of the MWCNT/TiO_2 core–shell structure. HRTEM results revealed that the core–shell structure of MWCNT/TiO_2 was constructed by the deposition of the TiO_2 nanoparticles along the tube wall of MWCNTs. The thickness of the TiO_2 shell layer was measured from the HRTEM images. The TiO_2 layer was found to have an average thickness of *ca.* 16.6 nm, calculated from repetitive measurements at various spots in the images (Fig. 3b). High magnification image (Fig. 3c) disclosed that the TiO_2 shell was composed of TiO_2 nanoparticles deposited on the tube wall. Heterojunction of the

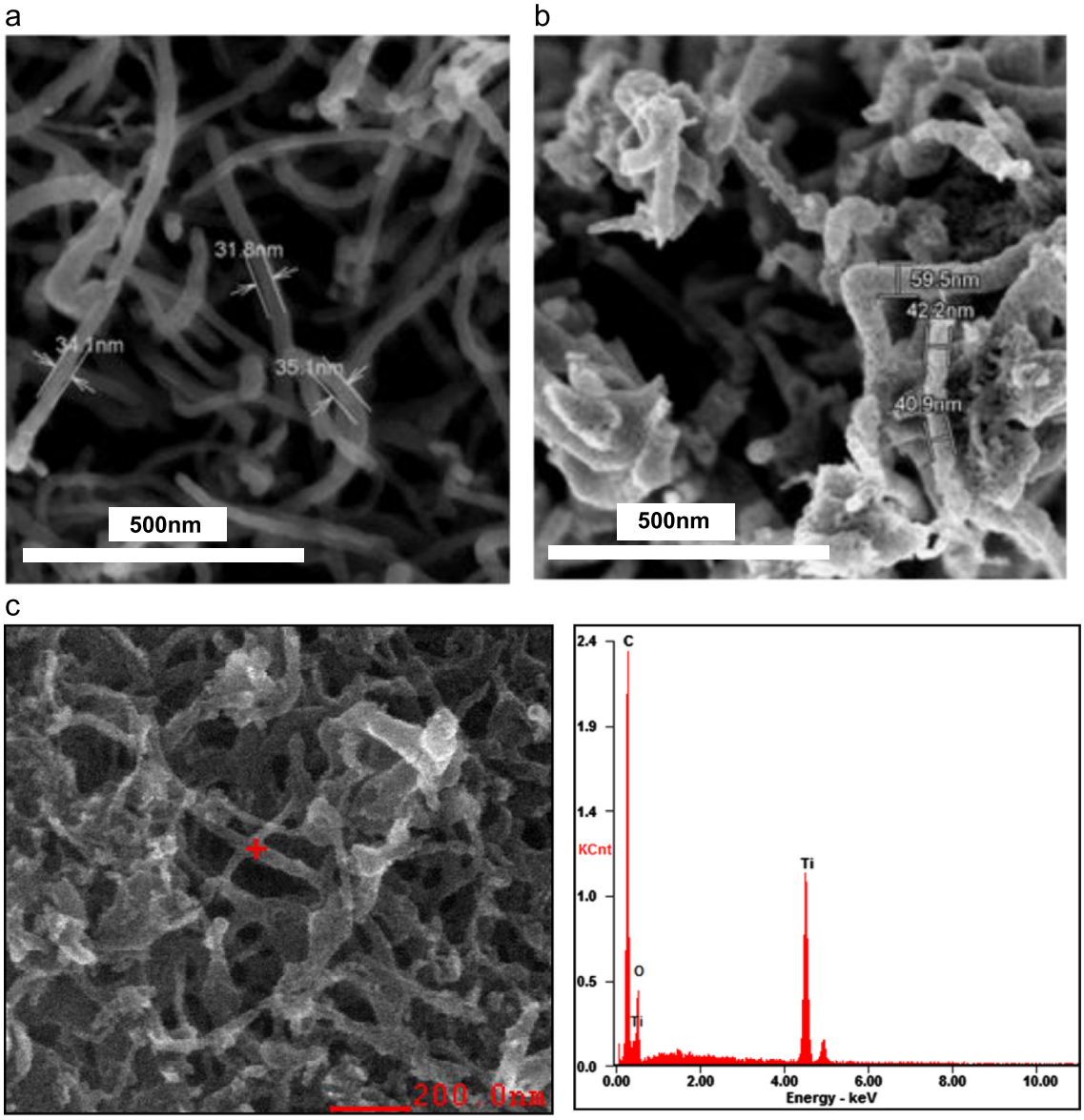

Fig. 2. FESEM images of (a) acid-treated MWCNTs, (b) MWCNT/TiO_2 core–shell nanocomposites and (c) EDS results on MWCNTs/TiO_2 structure.

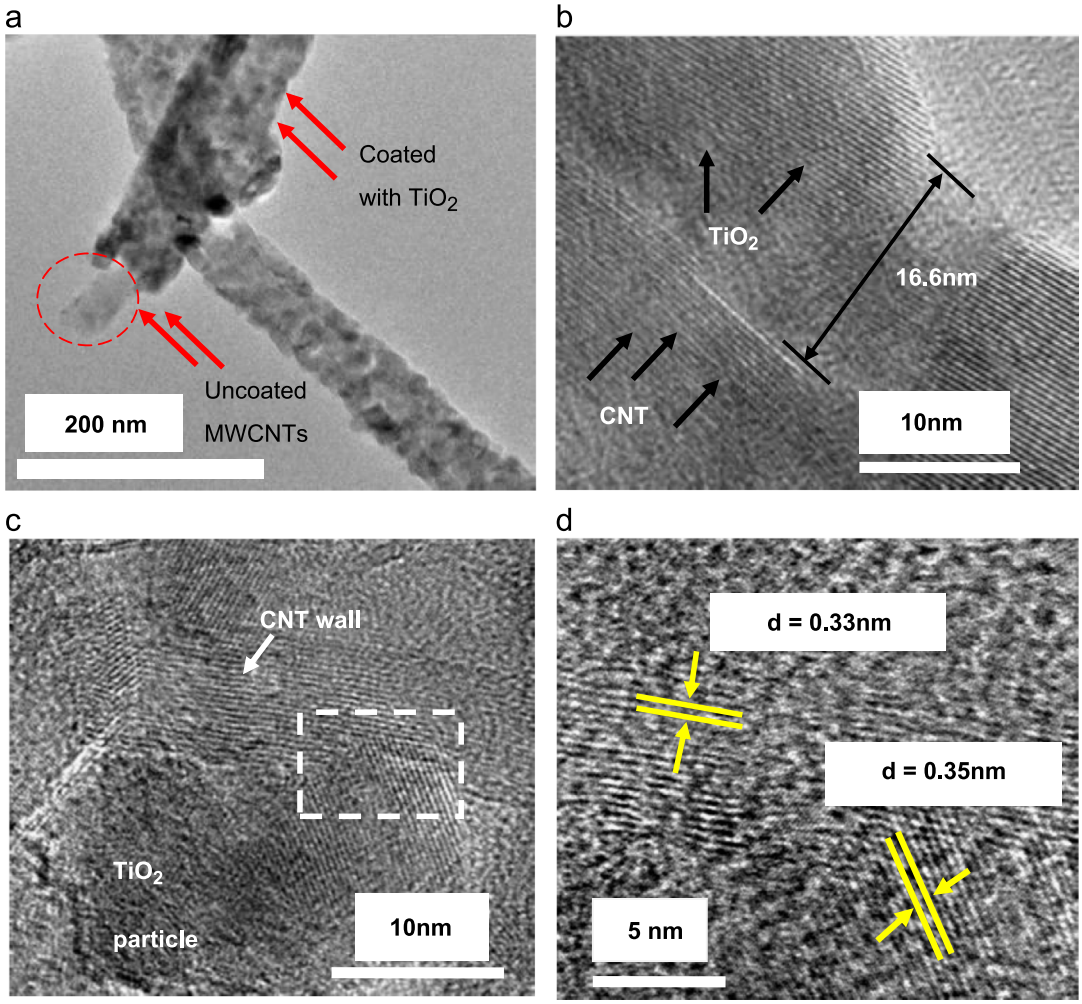

Fig. 3. HRTEM images of (a) the MWCNT/TiO_2 nanocomposites, ((b) and (c)) TiO_2 shell and (d) enlarged image of the selected MWCNT-TiO_2 heterojunction.

MWCNT-TiO_2 (highlighted area in Fig. 3c) can be significantly visualized from the overlapping of the two different lattice fringes of MWCNTs and TiO_2. The MWCNT-TiO_2 heterojunction would promote electron transfer between the two composites, thus, leading to red shift of the light absorption edge into visible region [23]. Fig. 3d shows the lattice fringes of the TiO_2 and MWCNT wall. The lattice spacing of *ca.* 0.35 nm obtained from the TiO_2 nanoparticles is attributed to the crystal facet of (1 0 1) [24]. Meanwhile, the lattice spacing of *ca.* 0.33 nm is identical to the facet of (0 0 2) of the MWCNTs [6,7].

XRD analysis was performed to examine the crystal phase of the nanocomposites. The peaks observed at 2θ=25.2°, 37.9°, 48.3°, 53.9°, 55.0°, 62.7°, 68.9°, 70.1°, and 75.5° were identified to be the anatase phase TiO_2 with various crystal structures as labeled in the spectrum shown in Fig. 4 [25]. The strongest diffraction was associated with the (1 0 1) facets, which indicates a much preferred crystallization of the deposited TiO2 along the (1 0 1) direction of the anatase phase. Rutile TiO_2 was not detected and it could be due to the relatively low calcination temperature (at 400 °C) employed in this work. The phase transformation of anatase into rutile phase would only begin at the temperatures above 550 °C [5]. The crystallite size of the TiO_2 nanoparticles was determined from Scherrer's equation using a *K* factor of cubic particles of 0.90. The TiO_2 was estimated to have the crystallite size of *ca.* 24.4 nm based on the strongest diffraction peak for the anatase (1 0 1) facets (Fig. 4).

Fig. 5 displays the Raman spectra of the MWCNT/TiO_2 nanocomposites and pristine MWCNTs. The Raman spectrum of

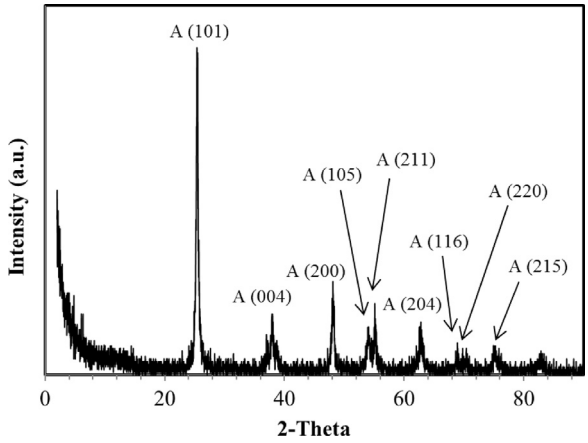

Fig. 4. XRD spectrum of MWCNT/TiO_2 core–shell nanocomposites. *A denotes as anatase.

MWCNT/TiO_2 nanocomposites exhibited characteristic peaks of anatase TiO_2 as well as *G*- and *D*-band of MWCNTs. Four characteristic peaks at the wavenumbers of *ca.* 155 cm^{-1} (E_g), 402 cm^{-1} (B_{1g}), 519 cm^{-1} ($B_{1g}+A_{1g}$) and 639 cm^{-1} (E_g) were observed, revealing that anatase was the predominant phase of the TiO_2 shell [26,27]. The crystal phase analysis by the Raman spectroscopy gave consistent result with the XRD in which no rutile and brookite phase TiO_2 was found. The characteristic

peaks of MWCNTs, *i.e.* *D*- and *G*-band, were observed at 1334 cm^{-1} and 1587 cm^{-1}, respectively in the MWCNT/TiO_2 nanocomposites, acid-treated MWCNTs and pristine MWCNTs. Asymmetric *G*-bands due to the formation of *G** bands were noticed at ~1600 cm^{-1} in the spectra of both the acid-treated MWCNTs and MWCNT/TiO_2 nanocomposites, which indicates the creation of defect sites on the MWCNT during the acid treatment [28]. The degree of graphitization (I_G/I_D) of the MWCNTs was found to reduce from 1.13 of the pristine MWCNTs to 0.70 of the acid-treated MWCNTs, which also uncovers that the defects were generated during the acid treatment. The I_G/I_D ratio of MWCNT/TiO_2 was determined to be 0.76, showing that TiO_2 coating did not cause significant defects to the MWCNT side wall.

3.2. Formation scheme of MWCNT/TiO_2 core–shell structure

The principle of the two-step synthesis of the MWCNT/TiO_2 core–shell structure is as illustrated in Scheme 1. The acid treatment was done to introduce hydrophilic behavior in the MWCNT surface *via* formation of carboxyl groups. The second step involved the dispersion of MWCNTs into water, followed by hydrolysis of titanium butoxide with water molecules which were readily attached to the surface of the MWCNTs, forming a layer of amorphous TiO_2 that covered the surface of the MWCNTs uniformly. The anatase TiO_2 shell with a preferred (1 0 1) orientation was subsequently obtained after calcination at 400 °C.

3.3. CO_2 photoreduction

CO_2 photoreduction was conducted to study the photocatalytic performance of the MWCNT/TiO_2 nanocomposites. Methane gas was detected in the product stream, which shows that CO_2 was successfully reduced to methane over the MWCNT/TiO_2 nanocomposites. The yield of methane upon the reaction is shown in Fig. 6. The MWCNT/TiO_2 nanocomposites exhibited superior photocatalytic activity as compared to the pure MWCNTs and anatase TiO_2. At the initial stage of the photoreaction, *i.e.* from 0 to 3 h, very low concentration of methane was detected. This observation may be attributed to the low photocatalytic activity at the beginning of the irradiation process, during which mainly intermediate products

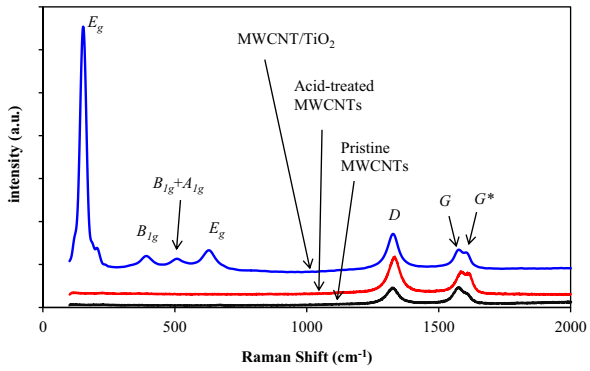

Fig. 5. Raman spectra of pristine MWCNTs, acid-treated MWCNTs, and MWCNT/TiO_2 nanocomposites.

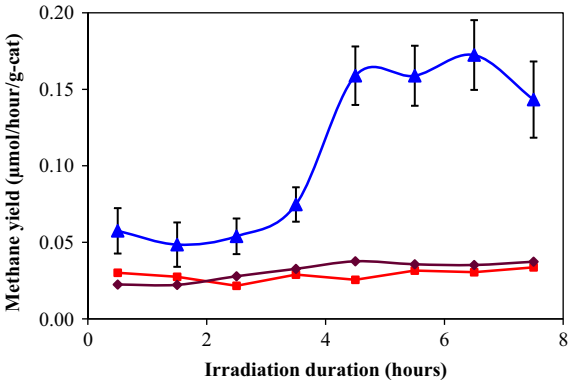

Fig. 6. Methane yields as a function of irradiation time: (▲) MWCNT/TiO_2 nanocomposites, (♦) MWCNTs, and (■)anatase TiO_2.

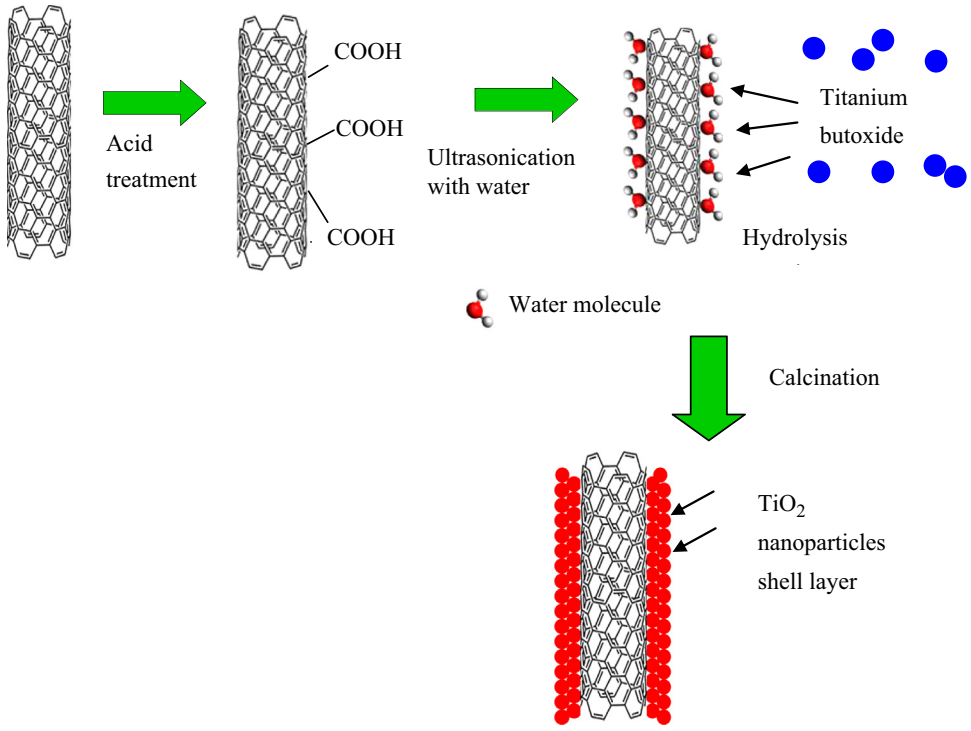

Scheme 1. Schematic of the proposed coating method.

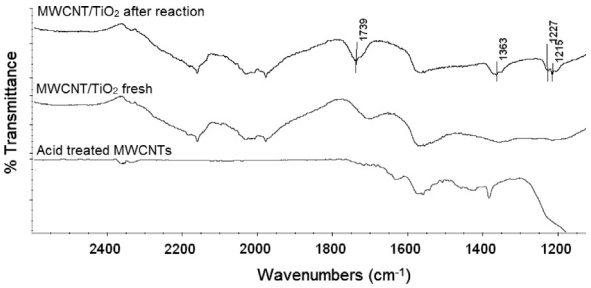

Fig. 7. FT-IR spectra of MWCNT/TiO_2 nanocomposites before and after the CO_2 photoreduction reaction.

such as radicals were evolved at this stage [22,29–31]. The yield of methane was found to increase with the irradiation duration, achieving its maximum yield of *ca.* 0.17 μmol/g-catalyst/h at the 6th hour of irradiation. Prolonging the photoreaction to a duration of more than 6 h reduced the catalytic activity probably due to saturation of the active sites by adsorbed intermediate products [30,32]. Very low methane yield was observed from the CO_2 photoreduction reactions conducted with the acid-treated MWCNTs and the anatase TiO_2. MWCNTs with defects after acid treatment have been also reported earlier to have a low photocatalytic activity [20,33]. The low activity of TiO_2 for the conversion of CO_2 into methane would be due to that only a small fraction of UV light was present in the light source of the reaction, indicated by its light absorption spectrum (Fig. S3, Supplementary materials).

Fig. 7 shows the FT-IR spectra of the MWCNT/TiO_2 nanocomposites after the CO_2 photoreduction as compared with the fresh MWCNT/TiO_2 nanocomposites and acid-treated MWCNTs. Three peaks observed at *ca.* 1739 cm^{-1}, 1363 cm^{-1}, and 1215–1227 cm^{-1} in the spectrum after the CO_2 photoreduction reaction were correspondent to the absorption of $\nu(CH_2{=}O)$ of formaldehyde, asymmetric CO_3 stretching vibration band, $\nu_{as}(CO_3)$, and C–O stretching of carbonyl group, respectively [34,35]. The presence of these intermediate products further confirms that CO_2 was converted to methane *via* the photocatalytic reduction with water.

3.4. Photoexcitation scheme of the MWCNT/TiO_2 core–shell structure

Upon the irradiation with visible light, TiO_2 underwent charge separation generating electron–hole pairs (Eq. (2)). The electron–hole pairs were separated and trapped at the surface vacancies and subsequently initiated the photoreduction reaction by reacting with CO_2 and water, in which water was oxidized with holes, generating oxygen and H^+ ions. CO_2 was reduced into methane by reaction with electrons, following the reactions as presented in Eqs. (3) and (4), respectively [36,37].

$$TiO_2 + h\nu \rightarrow TiO_2\,(e^-_{cb}) + TiO_2\,(h^+_{vb}) \quad (2)$$

$$2H_2O + 4h^+ \rightarrow 4H^+ + O_2 \quad (3)$$

$$CO_2 + 8H^+ + 8e^- \rightarrow CH_4 + 2H_2O \quad (4)$$

The electron charge transfer mechanism during the photoexcitation of the composites was investigated and proposed in Scheme 2. MWCNTs with their unique electrical and electronic properties played an important role to improve the electron charge transfer efficiency during the photoirradiation. Photogeneration and trapping of electron–hole pairs at the surface vacancies created non-equilibrium charging state between the TiO_2 and MWCNT. These trapped electrons would thus transfer from the conduction band (CB) of TiO_2 to the neighboring MWCNT which has lower band-edge position to achieve charge equilibrium

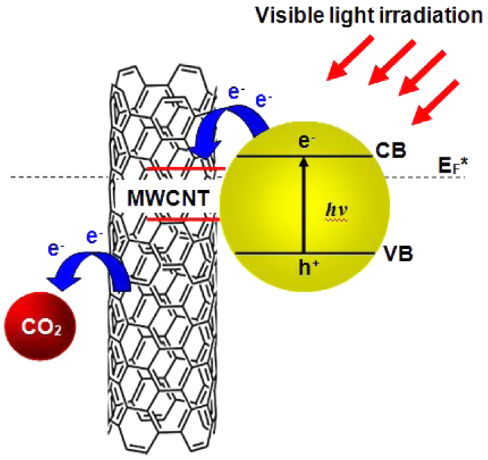

Scheme 2. Photoexcitation of the MWCNT/TiO_2 nanocomposites and the subsequent electron charge transfer.

in between these two semiconductors [7,37,38]. In addition, the transfer of electrons to MWCNT would reduce the trapping of electrons in the lattice of TiO_2, subsequently reduced the electron–hole recombination. This would generate more holes on the TiO_2 surface for the oxidation of water and H^+ ions for the reduction of CO_2, hence improved the overall efficiency of the photoreduction reaction.

4. Conclusions

MWCNT/TiO_2 core–shell nanocomposites with enhanced photoreactivity were successfully developed in this work. Uniform coating of TiO_2 overlayer on the surface of MWCNTs was obtained without any use of surfactant. We also demonstrated for the first time that the core–shell MWCNT/TiO_2 nanocomposites were photoactive for the reduction of CO_2 into methane under visible light irradiation. It is noteworthy that the maximum methane yield of *ca.* 0.17 μmol/g-catalyst/h was obtained at the 6th hour of reaction in a continuous CO_2 flow using an energy saving light bulb of low irradiation power (15 W). The photoexcitation mechanism suggests that the enhanced photoreactivity of these core–shell nanocomposites was achieved *via* electron transfer between the TiO_2 shell and the MWCNTs, which inhibited the electron–hole pair recombination and improved the overall efficiency of the photocatalysis.

Acknowledgements

The authors would like to thank the Ministry of Higher Education of Malaysia (LRGS, 2110226-113-00; FRGS/1/2013/TK05/MUSM/02/1) and Monash University Malaysia for the financial support given.

Appendix A. Supplementary materials

Supplementary data associated with this article can be found in the online version at http://dx.doi.org/10.1016/j.solmat.2013.11.034.

References

[1] G. Guan, T. Kida, A. Yoshida, Reduction of carbon dioxide with water under concentrated sunlight using photocatalyst combined with Fe-based catalyst, Appl. Catal., B 41 (2003) 387–396.

[2] X.-H. Xia, Z.-J. Jia, Y. Yu, Y. Liang, Z. Wang, L.-L. Ma, Preparation of multi-walled carbon nanotube supported TiO_2 and its photocatalytic activity in the reduction of CO_2 with H_2O, Carbon 45 (2007) 717–721.
[3] K. Woan, G. Pyrgiotakis, W. Sigmund, Photocatalytic carbon-nanotube–TiO_2 composites, Adv. Mater. 21 (2009) 2233–2239.
[4] W. Feng, Y. Feng, Z. Wu, A. Fujii, M. Ozaki, K. Yoshino, Optical and electrical characterizations of nanocomposite film of titania adsorbed onto oxidized multiwalled carbon nanotubes, J. Phys. Condens. Matter 17 (2005) 4361.
[5] N. Bouazza, M. Ouzzine, M.A. Lillo-Ródenas, D. Eder, A. Linares-Solano, TiO_2 nanotubes and CNT–TiO_2 hybrid materials for the photocatalytic oxidation of propene at low concentration, Appl. Catal., B 92 (2009) 377–383.
[6] J. Yu, T. Ma, S. Liu, Enhanced photocatalytic activity of mesoporous TiO_2 aggregates by embedding carbon nanotubes as electron-transfer channel, Phys. Chem. Chem. Phys. 13 (2011) 3491–3501.
[7] Y. Cong, X. Li, Y. Qin, Z. Dong, G. Yuan, Z. Cui, X. Lai, Carbon-doped TiO_2 coating on multiwalled carbon nanotubes with higher visible light photocatalytic activity, Appl. Catal., B 107 (2011) 128–134.
[8] Y. Yu, J.C. Yu, J.-G. Yu, Y.-C. Kwok, Y.-K. Che, J.-C. Zhao, L. Ding, W.-K. Ge, P.-K. Wong, Enhancement of photocatalytic activity of mesoporous TiO_2 by using carbon nanotubes, Appl. Catal., A 289 (2005) 186–196.
[9] L. Tian, L. Ye, K. Deng, L. Zan, TiO_2/carbon nanotube hybrid nanostructures: solvothermal synthesis and their visible light photocatalytic activity, J. Solid State Chem. 184 (2011) 1465–1471.
[10] D. Eder, A.H. Windle, Morphology control of CNT–TiO_2 hybrid materials and rutile nanotubes, J. Mater. Chem. 18 (2008) 2036–2043.
[11] D. Wang, L. Xiao, Q. Luo, X. Li, J. An, Y. Duan, Highly efficient visible light TiO_2 photocatalyst prepared by sol–gel method at temperatures lower than 300 °C, J. Hazard. Mater. 192 (2011) 150–159.
[12] D. Eder, I.A. Kinloch, A.H. Windle, Pure rutile nanotubes, Chem. Commun. (2006) 1448–1450.
[13] H. Wang, H.-L. Wang, W.-F. Jiang, Solar photocatalytic degradation of 2, 6-dinitro-*p*-cresol (DNPC) using multi-walled carbon nanotubes (MWCNTs)–TiO_2 composite photocatalysts, Chemosphere 75 (2009) 1105–1111.
[14] Y. Ou, J. Lin, S. Fang, D. Liao, MWNT–TiO_2:Ni composite catalyst: a new class of catalyst for photocatalytic H_2 evolution from water under visible light illumination, Chem. Phys. Lett. 429 (2006) 199–203.
[15] W.-J. Ong, M.M. Gui, S.-P. Chai, A.R. Mohamed, Direct growth of carbon nanotubes on Ni/TiO_2 as next generation catalysts for photoreduction of CO_2 to methane by water under visible light irradiation, RSC Adv. 3 (2013) 4505–4509.
[16] F. Wang, K. Zhang, Physicochemical and photocatalytic activities of self-assembling TiO_2 nanoparticles on nanocarbons surface, Curr. Appl. Phys. 12 (2012) 346–352.
[17] W. Zhou, K. Pan, Y. Qu, F. Sun, C. Tian, Z. Ren, G. Tian, H. Fu, Photodegradation of organic contamination in wastewaters by bonding TiO_2/single-walled carbon nanotube composites with enhanced photocatalytic activity, Chemosphere 81 (2010) 555–561.
[18] W.-M. Yeoh, K.-T. Lee, A.R. Mohamed, S.-P. Chai, Production of carbon nanotubes from chemical vapor deposition of methane in a continuous rotary reactor system, Chem. Eng. Commun. 199 (2012) 600–607.
[19] SPI-Chem Polyethylene Glycol 200, in: ⟨http://www.2spi.com/catalog/chem/poly.php⟩. Accessed date: 23rd August 2013.
[20] C.G. Silva, L.F. Joaquim, Photocatalytic oxidation of benzene derivatives in aqueous suspensions: synergic effect induced by the introduction of carbon nanotubes in a TiO_2 matrix, Appl. Catal., B 101 (2010) 81–89.
[21] S. Wang, et al., Preparation, characterization and photocatalytic activity of multi-walled carbon nanotube-supported tungsten trioxide composites, J. Phys. Chem. Solids 69 (2008) 2396–2400.
[22] Slamet, H.W. Nasution, E. Purnama, S. Kosela, J. Gunlazuardi, Photocatalytic reduction of CO_2 on copper-doped titania catalysts prepared by improved-impregnation method, Catal. Commun. 6 (2005) 313–319.
[23] S. Qin, F. Xin, Y. Liu, X. Yin, W. Ma, Photocatalytic reduction of CO_2 in methanol to methyl formate over CuO–TiO_2 composite catalysts, J. Colloid Interface Sci. 356 (2011) 257–261.
[24] Q. Zhang, Y. Li, E.A. Ackerman, M. Gajdardziska-Josifovska, H. Li, Visible light responsive iodine-doped TiO_2 for photocatalytic reduction of CO_2 to fuels, Appl. Catal., A 400 (2011) 195–202.
[25] Q.-H. Zhang, W.-D. Han, Y.-J. Hong, J.-G. Yu, Photocatalytic reduction of CO_2 with H_2O on Pt-loaded TiO_2 catalyst, Catal. Today 148 (2009) 335–340.
[26] P. Falaras, A. Hugot-Le Goff, M.C. Bernard, A. Xagas, Characterization by resonance Raman spectroscopy of sol–gel TiO_2 films sensitized by the Ru $(PPh_3)_2$(dcbipy)Cl_2 complex for solar cells application, Sol. Energy Mater. Sol. Cells 64 (2000) 167–184.
[27] T. Ohsaka, F. Izumi, Y. Fujiki, Raman spectrum of anatase, TiO_2, J. Raman Spectrosc. 7 (1978) 321–324.
[28] R. Graupner, Raman spectroscopy of covalently functionalized single-wall carbon nanotubes, J. Raman Spectrosc. 38 (2007) 673–683.
[29] K. Kočí, K. Matějů, L. Obalová, S. Krejčíková, Z. Lacný, D. Plachá, L. Čapek, A. Hospodková, O. Šolcová, Effect of silver doping on the TiO_2 for photocatalytic reduction of CO_2, Appl. Catal., B 96 (2010) 239–244.
[30] S.S. Tan, et al., Photosynthesis of hydrogen and methane as key components for clean energy system, Sci. Technol. Adv. Mater. 8 (2007) 89.
[31] O. Ozcan, F. Yukruk, E. Akkaya, D. Uner, Dye sensitized CO_2 reduction over pure and platinized TiO_2,, Top. Catal. 44 (2007) 523–528.
[32] N. Sasirekha, S.J.S. Basha, K. Shanthi, Photocatalytic performance of Ru doped anatase mounted on silica for reduction of carbon dioxide, Appl. Catal., B 62 (2006) 169–180.
[33] Y. Luo, Y. Heng, X. Dai, W. Chen, J. Li, Preparation and photocatalytic ability of highly defective carbon nanotubes, J. Solid State Chem. 182 (2009) 2521–2525.
[34] H. Tsuneoka, K. Teramura, T. Shishido, T. Tanaka, Adsorbed species of CO_2 and H_2 on Ga_2O_3 for the photocatalytic reduction of CO_2, J. Phys. Chem. C 114 (2010) 8892–8898.
[35] N. Ulagappan, H. Frei, Mechanistic study of CO_2 photoreduction in Ti silicalite molecular sieve by FT-IR spectroscopy, J. Phys. Chem. A 104 (2000) 7834–7839.
[36] Y. Li, W.-N. Wang, Z. Zhan, M.-H. Woo, C.-Y. Wu, P. Biswas, Photocatalytic reduction of CO_2 with H_2O on mesoporous silica supported Cu/TiO_2 catalysts, Appl. Catal., B 100 (2010) 386–392.
[37] A. Kongkanand, P.V. Kamat, Electron storage in single wall carbon nanotubes. Fermi level equilibration in semiconductor—SWCNT suspensions, ACS Nano 1 (2007) 13–21.
[38] T. Tsubota, A. Ono, N. Murakami, T. Ohno, Characterization and photocatalytic performance of carbon nanotubes material-modified TiO_2 synthesized by using the hot CVD process, Appl. Catal., B 91 (2009) 533–538.